JOURNAL OF GEOPHYSICAL RESEARCH, VOL. ???, XXXX, DOI:10.1029/,

Source Location of the Wedge-like Dispersed Ring Current in the Morning Sector During a Substorm

M. Yamauchi,[1] P. C. Brandt,[2] Y. Ebihara,[3] I. Dandouras,[4] H. Nilsson,[1] R. Lundin,[1] H. Rème,[4] C. Vallat,[5] P.-A. Lindquvist,[6] A. Balogh,[7] and P.W. Daly[8]

Abstract. Source of wedge-like dispersed sub-keV ring current ions (wedge-like structure) is investigated using Cluster CIS data. Statistics from nearly

---

A. Balogh, Blackett Laboratory, Imperial College London, London SW7 2BW, UK (a.balogh@imperial.ac.uk)

P. C. Brandt, Johns Hopkins University Applied Physics Laboratory, Laurel, MD 20723-6099, USA (pontus.brandt@jhuapl.edu)

P.W. Daly, Max-Planck Institut fuer Sonnensystemforschung, Max-Planck-Str. 2, 37191 Katlenburg-Lindau, Germany (daly@mps.mpg.de)

I. Dandouras and H. Rème, Centre d'Etude Spatiale des Rayonnements, BP 4346, 31028 Toulouse Cedex 4, France (Iannis.Dandouras@cesr.fr, Henri.Reme@cesr.fr)

Y. Ebihara, National Institute of Polar Research, 1-9-10 Kaga, Itabashi-ku, Tokyo 173-8515, Japan (ebihara@nipr.ac.jp)

P.-A. Lindquvist, Alfvén Laboratory, Royal Institute of Technology, SE-10044 Stockholm, Sweden (per-arne.lindqvist@alfvenlab.kth.se)

R. Lundin, H. Nilsson, and M. Yamauchi, Swedish Institute of Space Physics, Box 812, SE-98128 Kiruna, Sweden (Rickard.Lundin@irf.se, Hans.Nilsson@irf.se, M.Yamauchi@irf.se)

C. Vallat, ESA/ESTEC, RSSD SCI-SH, Keplerlaan 1, 2201 AZ Noorwijk ZH, The Netherlands (cvallat@rssd.esa.int)

[1]IRF, Kiruna, Sweden

[2]JHU/APL, Laurel, MD, USA

[3]NIPR, Tokyo, Japan

550 traversals show that the wedge-like structure with upper energy extending to ordinary energy of ring current is found mostly in the morning sector whereas those limited within sub-keV range are found mostly in the noon-to-afternoon sector. The former is most likely the original form of the latter. With this knowledge, the Cluster traversal on 21 October 2001 turned out to be a unique observation that reveals the formation of the wedge-like structure. Spacecraft 1 and 4 detected a wedge-like structure of 0.1 $\sim$ 10 keV protons at 23:50 UT, while spacecraft 3 did not detect it 10 minutes before in the same magnetic flux tube. With the observed electric field of less than 3 mV/m, this fact indicates that the dispersion started within half an hour. Pitch angle distributions of the wedge-like structure is in most cases double conic-like butterfly distributions, but the wedge-like dispersed oxygen ions during the 21 October 2001 event flow mainly from one direction (from northern hemisphere) without a loss cone. With its characteristic energy of 0.05 $\sim$ 0.3 keV, these oxygen ions originate from the northern hemisphere about

[4]CESR, Toulouse, France

[5]ESA/ESTEC, Noorwijk, The Netherlands

[6]Alfvén Lab., KTH, Stockholm, Sweden

[7]Blackett Lab., ICL, London, UK

[8]MPS, Katlenburg-Lindau, Germany

$20 \sim 30$ minutes before the observation. Both the dispersion analysis and the oxygen ion tracing suggest that the observed wedge-like structure is formed in the late morning sector during the latest substorm that started at 23:10 UT. Possible mechanisms of the morning source are discussed.

2778 Ring current. 2790 Substorms. 2730 Inner magnetosphere. 2760 Plasma convection. 7807 Charged particle motion and acceleration.

1. Introduction

Satellites traversing inside dayside ring current region frequently detect dense trapped sub-keV ions far equatorward of the auroral region [*Sauvaud et al.*, 1981; *Newell and Meng*, 1986; *Yamauchi et al.*, 1996a, 2005; *Ebihara et al.*, 2001]. These trapped ions are energy–latitude dispersed in mostly wedge-like forms [*Yamauchi et al.*, 1996a]. Figure 1a shows a Viking example (mid-altitude at 5000 $\sim$ 13000 km) and Figure 1b shows a Cluster example (high-altitude and L>4). In both examples, one can recognize an isolated plasma region in the sub-keV range as indicated by arrows at low latitude (low-L) side of the structured keV ions. One can also recognize that this isolated dense plasma region has several wedge-like energy dispersions overlapping each other, but the entire region is clearly separated in energy range from the ordinary (>5 keV) component of the ring current ions. Although the separation is clearer in the postnoon sector than in the morning sector according to the Viking observations (both Figures 1a and 1b are postnoon traversals), this population is predominantly found at morning-to-prenoon sectors [*Yamauchi et al.*, 2005], and thus has a different local-time distribution from the ordinary ring current component [e.g., *Collin et al.*, 1993].

Unfortunately, the sub-keV component of the ring current ions is not as well studied as the ordinary >5 keV component, partly because the total energy flux of 0.05 $\sim$ 1 keV ions is smaller than that of >5 keV ions in the ring current region, and partly because the dispersion pattern is so various that it is difficult to understand all the patterns. Yet, some independent satellite data analyses have demonstrated that the sub-keV component of the ring current dynamically changes in response to past substorm activities. Using

the Aureol-1 satellite (altitude 400 $\sim$ 2500 km), *Sauvaud et al.* [1981] demonstrated that sub-keV ion precipitation in the subauroral region increases some hours after substorm injection in the early morning (00-06 MLT) sector. Using the low-altitude DMSP F6 and F7 satellites, *Newell and Meng* [1986] demonstrated that sub-keV ion precipitation in the late morning (0830 MLT) subauroral region is strongly correlated with the Kp index with some hours of time delay, and the enhanced precipitation may last a day. Using the Viking satellite, *Yamauchi and Lundin* [2006] statistically showed that these wedge-like dispersed sub-keV ions are related to the past AE activity, but are not directly related to the past or present Dst activity although they are located in the ring current region.

The relation to the substorm is also indicated from particle-drift theory [*Ebihara et al.*, 2001], which was originally used to explain the energy–latitude dispersion pattern. The $\mathbf{E} \times \mathbf{B}$ drift (electric field E is the summation of the corotation field and external (dawn-to-dusk) magnetospheric field in this paper) is energy independent but local-time dependent because the $\mathbf{E} \times \mathbf{B}$ drift by the magnetospheric electric field generally points sunward, reinforcing the eastward corotation in the dawn sector and against it in the dusk sector. The competing westward gradient-$|B|$/curvature drift, which is energy dependent, is nearly local-time independent compared to the $\mathbf{E} \times \mathbf{B}$ drift.

In the region where the $\mathbf{E} \times \mathbf{B}$ drift is eastward (nearly at all local times except the dusk sector), the $\mathbf{E} \times \mathbf{B}$ drift and the gradient-$|B|$/curvature drift balance each other at a certain energy above which the ions drift westward and below which the ions drift eastward. For ions with energies below this threshold energy, the eastward drift is faster for the lower energy ions than for the higher energy ions. Since the total drift velocity is

different for different L shells [e.g., Table 2 of *Yamauchi and Lundin*, 2006], this causes the energy–latitude dispersion reported by *Yamauchi et al.* [1996a].

Along this scenario, *Ebihara et al.* [2001] made a particle-drift simulation using up to second order invariant conservation for both the $\mathbf{E} \times \mathbf{B}$ drift (energy independent) and gradient-$|B|$/curvature drifts (westward for positive ions, energy dependent). The simulation assumed a bursty (order of tens of minutes) injection of Maxwellian plasma from the nightside, presumably during substorms, into the dipole-like magnetic field region. The simulation successfully reconstructed the three main patterns of wedge-like energy–latitude dispersions as well as the local-time dependence observed by Viking (high probability in the morning and decreasing with local time in the dayside [*Ebihara et al.*, 2001; *Yamauchi et al.*, 2005]). With this successful explanation, we hereafter call the wedge-like energy–latitude dispersed sub-keV ions in the ring current region the "wedge-like structure."

To examine more precisely the relation between the wedge-like structures and substorm activities, *Yamauchi and Lundin* [2006] made a statistical study of over 700 Viking dayside traversals using backward superposed epoch analyses. This work confirmed that the wedge-like structures in the dayside are formed during the substorm activities monitored by hourly-AE, and they drift eastward while decaying with a time scale comparable to the charge-exchange decay. This result means that studying the wedge-like structure provides a good clue in understanding the dynamics of the inner magnetosphere after substorms.

While the transport of the wedge-like structures is qualitatively understood, our previous studies also found unexpected results related to the source location and the transport mechanisms.

1. The source population of the wedge-like structure is most likely generated in a wide local-time range from early morning to pre-midnight. The early morning sector could be the largest source because the structure appears in the morning sector (5-7 MLT) within $0 \sim 2$ hours after high AE activities [*Yamauchi and Lundin*, 2006]. The formation mechanism of the source population is unsolved at present [*Ebihara et al.* 2001].

2. The wedge-like structure drifts slightly faster to the eastward than predicted by simple models. It drifts even to the afternoon sector beyond what the models predict. The structures seen in the evening sector most likely have traveled from the morning sector by eastward drift rather than directly from the nightside by westward drift [*Yamauchi and Lundin*, 2006].

3. While the wedge-like structures observed by Viking are clearly spatial structures (we compared ascending and descending traversals), Cluster observations quite often show inbound-outbound asymmetry in the dispersion direction, indicating a substantial temporal effect, i.e., the traversal time of Cluster across the ring current region (one to few hours) can no longer be ignored compared to the drift time of the wedge-like structure [*Yamauchi et al.*, 2005]. This is another support for the Viking result that the drift speed is faster than simple model predictions.

4. While the wedge-like structure at low-altitude (Freja) is mainly composed of oxygen ions (O^+), it is mainly composed of protons (H^+) at high-altitude (Cluster) [*Yamauchi et al.*, 2005]. This suggest that the O^+ might be generated in a different way from H^+, e.g. by sputtering from energetic ring current [Yamauchi et al., 1996a].

5. The peak occurrence probability in the Cluster data is found in the noon-to-postnoon sector, which is somewhat inconsistent with other satellites (Freja and Viking) or with the

model [*Yamauchi et al.*, 2005]. The inconsistency is mainly attributed to lower occurrence probability by Cluster than by Viking or simulation in the morning sector. Although the Cluster satellites cover down to only L >4, this is enough to cover the majority of the wedge-like structures in the dayside [*Yamauchi and Lundin* 2006]. The discrepancy therefore indicates that the identification criterion in [*Yamauchi et al.* [2005] was probably inappropriate for Cluster.

The major new finding by the past observations is the first point, i.e., the dispersion may have started in the morning sector for a substantial number of cases. In other words, the major unanswered problem on the wedge-like structure is its formation (location, timing, and mechanism) during the substorms. However, before attacking this problem, we have to first solve the last problem listed above, i.e. the identification of the high-altitude signature of the wedge-like structure (particularly in the morning sector).

In this paper, we first re-examine the Cluster CIS data with a generalized criterion for identification of wedge-like structures, and show that the new criterion produces the same local-time dependence as for the Viking observations and simulations. The refined Cluster statistics helps in searching cases in which we can see the sudden appearance of the wedge-like structure during a single perigee traversal of Cluster. The Cluster perigee traversal during 21–22 October 2001 showed a unique example in the three-year statistics for such a sudden appearance, and we report it.

2. Cluster Statistics

The CIS (Cluster Ion Spectrometry) experiment is a comprehensive ion plasma spectrometry package onboard the four Cluster spacecraft, capable of obtaining full three-dimensional ion distributions with good time resolution (one spacecraft spin) and with

mass-per-charge composition determination. The CIS package consists of two different instruments, a Hot Ion Analyser (HIA) and a time-of-flight ion Composition Distribution Function (CODIF), plus a data processing system (DPS) that permits extensive onboard data processing. The instrument works on three spacecraft (S/C-1, S/C-3, and S/C-4). For detailed description of the instrument, refer to *Rème et al.* [2001]. We use CODIF data for our analyses.

2.1. Event Identification

Figure 2 shows three examples of the wedge-like structure observed by CIS around its perigee. In the top panel of Figure 2a, the wedge-like structure is easily identified as is indicated by the arrow. Similar energy–time dispersed stripes can be recognized in Figure 2b, but the energy range of the stripes extends to higher energies than those in Figure 2a, and the upper envelope (in energy) of the dense plasma region in Figure 2b has a band-like flat energy, while the envelope is a round shape in Figure 2a. A further modification of the dispersion pattern is recognized in Figure 2c: it is similar to Figure 2b except that the visible stripes are nearly dispersion-free in Figure 2c.

In *Yamauchi et al.* [2005], we identified such low-energy dense plasma as wedge-like structures only if the dense sub-keV ring current ions are found inside the cavity in energy space as shown in Figure 2a (i.e., the empty region bounded by the ordinary ring current ions at >10 keV range). We did not include cases as the wedge-like structures when such a separation is not clear like in the examples of Figures 2b or 2c, to avoid mixing with the ion signatures of the auroral region. Another reason for such a restrictive criterion is because the sub-keV component was clearly separated from the energetic (>5 keV) component in the energy–pitch angle distribution in the CRRES statistics [*Collin*

et al., 1993]. However, a separation in a statistical average does not necessarily mean a separation at this average energy for an individual case. Therefore, the criterion requiring inside the cavity could be too restrictive, and could be the reason for the inconsistency in the local time distribution between the Cluster result and the Viking/simulation results.

The separation energy, or sometimes called gap energy [*Vallat*, 2004]], is theoretically expected to be local-time dependent. As mentioned in the introduction, the $\mathbf{E} \times \mathbf{B}$ drift (mostly points eastward) and the westward gradient-$|B|$/curvature drift balance with each other at a certain energy, and this threshold energy varies with local time. Since the eastward ($\mathbf{E} \times \mathbf{B}$) drift in the dayside decrease with local time while the competing westward drift is nearly local-time independent, the upper threshold energy of the eastward drift (i.e., upper energy cut off of the wedge-like structure) decreases with local time. Note that the convection electric field varies dynamically, and hence the threshold energy varies in time depending on the magnetospheric activity.

On the other hand, the westward drifting ordinary (high-energy) ring current ions have to overcome the corotation to reach the dayside via westward route (the corotation electric field is larger than the magnetospheric (dawn-to-dusk) electric field in dayside). Since both the corotation and the westward magnetic drift are local time independent, the lower energy cutoff of the ordinary ring current becomes nearly constant in the dayside. As a total, the energy gap between the energetic component and the sub-keV component is wider in the afternoon sector than in the morning sector. This tendency is seen in the simulation result by *Ebihara et al.* [2001]. In fact, the Cluster traversals with the gap energy around one to few keV, which corresponds to a clear cavity in energy space, are mostly found in the afternoon sector [*Vallat*, 2004 (see their Figure 3-19)].

With this background knowledge, the overall morphologies of Figure 2a (noon, non-storm time) and Figure 2b (3 LT, non-storm time) seem to have a gradual transition corresponding to the local-time dependence, and have a common generation process. Therefore, we might extend the criterion to allow cases like Figure 2b, i.e., a partial overlap between the low energy component and high energy component at their high latitude parts. The difference between Figure 2b (3 LT, non-storm time) and Figure 2c (6 LT, storm time) is just the strength of the dispersion, which strongly depends on the drift distance and the electric field strength. If we include Figure 2b as the wedge-like structure, it is natural to include Figure 2c. Therefore, we introduce a new criterion that allows us to include the cases shown in Figures 2b and 2c as wedge-like structures.

To compare with the previous result by *Yamauchi et al.* [2005], we take a statistics with two categories when re-analyzing the CIS/CODIF data: the clear wedge-like structure with upper energy limited to about 1 keV (Figure 2a, and we call it "limited wedge-like structure"); and the one with upper energy extending to a higher energy while starting from sub-keV (Figures 2b or 2c, and we call it "extended wedge-like structure"). The classification is done by eye-identification from the energy–time spectrogram of the ion energy flux which is scaled with $10^{5\sim7}$ keV·cm^{-2}s^{-1}keV^{-1}.

As described in *Yamauchi and Lundin* [2006], it is inadequate (and impossible) to make an automated identification algorithm to classify the wedge-like structure. To show the rough accuracy of the eye-identification method, we added the "weak" category that is difficult to classify as a wedge-like structure but still shows significant flux in the right energy interval. The peak energy flux of the weak category is about $3{\cdot}10^5$ keV·cm^{-2}s^{-1}keV^{-1}. Probability of this category gives a good estimate of error bar.

In this paper, we do not sub-classify the wedge-like structure in terms of the dispersion direction as we did in *Yamauchi et al.* [2005] because the dispersion direction observed by Cluster reflects the temporal change as mentioned in the introduction (in fact both Figure 2a and 2b show increasing energy in time for both inbound traversal and outbound traversal).

2.2. Result

Figure 3 shows the probability of observing the wedge-like structures obtained from 552 inbound/outbound traversals to/from the perigee (over 300 orbits) during two and half years (January 2001 – July 2003). The extended wedge-like structure has a probability peak in the morning sector and the limited wedge-like structure has a probability peak in the afternoon sector, with a smooth transition of the occurrence probabilities from one to the other as the local time increases. The total probability in Figure 3 shows the same local-time distribution as that for the wedge-like structure observed by Viking. The weak category does not significantly affect this result except an additional minor peak at 15 MLT only. Such an one-point minor peak is easily attributed to the uncertainty of the statistics.

Note that the matching of local-time distributions between Cluster and Viking is expected only if the majority of the wedge-like structures observed by Cluster are also observable by Viking. In Figure 2, the sub-keV stripes have a butterfly distribution (double conic-like distribution) with a sufficient parallel component to reach the Viking altitude in the geomagnetic mirror configuration. We have not made solid statistics, but the majority of the identified stripe structures (all types of Figures 2a, 2b, and 2c) show such butterfly distributions or trapped distributions with a very narrow loss cone ($<20^\circ$) while

the energetic (ordinary ring current) component shows simple trapped distribution with a relatively large loss cone. Thus the pitch angle distribution support the consistency in the local-time distribution between Cluster and Viking, and hence support our new criterion to include the extended wedge-like structure. This result confirms that the wedge-like structure observed by Cluster is also a fossil remnant of past substorm-related energization as is confirmed by Viking studies and simulations [*Ebihara et al.*, 2001; *Yamauchi and Lundin*, 2006].

Figure 3 also indicates that the extended wedge-like structure is most likely the original form of the limited wedge-like structure because the wedge-like structure in the dayside drifts eastward (this is demonstrated both by Viking data analyses [*Yamauchi and Lundin*, 2006] and simulation [*Ebihara et al.*, 2001]). In other words, the morphology of the wedge-like structure changes as the structure drifts eastward, from the shape shown in Figure 2b to the shape shown in Figure 2a. Such local-time dependence of the upper energy cutoff of the wedge-like structure is also seen in the Viking data [*Yamauchi and Lundin*, 2006, Figure 7].

Finally, Figure 3 shows that the probability of observing the extended wedge-like structure quickly decreases from the morning to the midnight. Considering its eastward motion mentioned above, and considering the general destination of the substorm injection [*McIlwain*, 1974] which mostly peaks in the midnight sector, we have three possibilities to explain the morning peak of the probability: (A) the wedge-like structure is formed in the midnight sector, but it is not detected due to the satellite orbital limit (detection limit effect); (B) the keV ions are formed in the midnight sector, but the plasma drifts very fast until reaching the morning sector so that the observation probability per unit MLT

is decreased (compression effect); and (C) the source keV ions are formed in the morning sector (local generation). The detail of each possibility is discussed in section 4.1.

3. The October 21, 2001 event

As is shown in the previous section, both Viking and Cluster statistics show that the probability of observing the wedge-like structures has a common local-time dependence with a morning peak. The Cluster statistics (Figure 3) further indicates that the dispersion might start in the morning sector for a substantial amount of cases, although the formation location of the original stripe population is not clear. What we need next is to find an example in which the sudden formation of the wedge-like structure is detected during a substorm. This work naturally requires multi-spacecraft data that can derive the drift distance.

3.1. Identification

Since the required case-study must observe a substorm-related sudden change of sub-keV ion density, and since the northern hemisphere and the southern hemisphere have basically the same plasma signature at a given local time and L-value in the dayside inner magnetosphere due to the mirror bouncing, we search Cluster perigee traversals (which is along nearly the same local time) with the most prominent north-south asymmetry. During the first three years of Cluster/CIS observation, the most prominent inbound-outbound asymmetry of the wedge-like structure is observed during the perigee traversal at around the midnight UT between 21 and 22 October 2001 during a large magnetic storm. Figure 4 shows the overall particle data of this event (4 hours). Figure 5 shows expanded data (50 minutes) with the pitch angle–time spectrograms for both oxygen ions

and protons. The magnetic local time (MLT) is around 9 MLT for all three spacecraft, and the inbound (south) and the outbound (north) are less than 1 hour apart in MLT.

In Figure 4, one can recognize a strong inbound-outbound asymmetry with series of intensive stripes extending from sub-keV to >10 keV only during the outbound traversal after 23:50 UT. During this period with intensive stripes, bursty stripes are recognized even in the energetic proton channel of the RAPID instrument. Among these stripes, only the first stripe (at around 23:50 UT for S/C-1 and S/C-4 and at around 00:00 UT for S/C-3) is clearly energy-dispersed starting from <0.1 keV to >10 keV. This first stripe shows a butterfly pitch angle distribution, particularly for the sub-keV part, according to Figure 5. Therefore, this is classified as an extended wedge-like structure. The start of this wedge-like structure is during the outbound traversals for S/C-1 and S/C-4, while it is near the perigee for S/C-3.

The spacecraft trajectory is illustrated in Figure 6. S/C-1 is ahead of S/C-4 by less than 5 minutes and S/C-3 is about half an hour after the other spacecraft. All spacecraft traversed nearly the same MLT sector (only a few degrees difference) during the time when the wedge-like structure appeared at 23:50–00:05 UT. The butterfly pitch angle distribution of the wedge-like structure guarantees filling of sub-keV protons along the same magnetic tube, and hence guarantees the north-south symmetry at the Cluster altitude.

From this orbital characteristics, the sudden and simultaneous appearance of both the wedge-like structure and >100 keV proton stripes only in the outbound traversal is extremely difficult to be explained by the spatial structure (we have to assume very sharp gradient). Instead, it is most likely caused by the temporal change during the perigee

traversal. On the other hand, the dispersion itself may reflect both the spatial structure and the temporal change.

The subsequent stripes seen after the wedge-like structure are vertical, i.e., with very little or no dispersion. The qualitative difference between the first stripe and the subsequent stripes is also seen in the RAPID data (Figure 4) in which the flux of >30 keV proton gradually decreases during the first stripe, whereas the dispersion-free stripes are synchronized with the sudden increases of >30 keV proton flux for the rest. These increases of >30 keV protons after the second stripe are accompanied by decreases of >30 keV electrons (not shown here). A decrease of the ordinary ring current component (>10 keV) is also recognized in both the proton spectrogram and the oxygen ion spectrogram at 23:50 UT.

The initial decrease of the ordinary ring current component at around 23:50 UT can be explained by the drift direction. Particles with energy greater than 10 keV apparently drifted westward before 23:50 UT, whereas this westward drift ceased afterward and the eastward drift started for the energy range <20 keV instead. The newly imposed electric field contributes to such a decrease of the energetic component. This explanation, however, does not work the subsequent stripes. With such qualitative differences between the first stripe and the subsequent stripes, we focus on this first wedge-like structure with strong dispersion. The subsequent stripes are discussed in subsection 4.2.

One may also notice a minor extra wedge-like structure only at $1 \sim 10$ keV range at around 23:50 UT in S/C-3. At that timing, the proton data from the other spacecraft also show a hanging structure from higher energy, while the wedge-like structure seen in the oxygen data is starting from the low-energy side. The wedge-like structure observed by

S/C-1 and S/C-4 at around 23:50 UT might correspond to those observed at around 23:50 UT by S/C-3 instead of those observed at around 00:00 UT (S/C-3), although the overall morphology (dispersed intense stripe followed by dispersion-free stripes) is the same as the latter. Because of this uncertainty, we make our whole discussion independent of the 00:00 UT event in the remainder of the paper so that our analysis does not depend on the relationship between the 23:50 UT event and the 00:00 UT event.

3.2. Analyses of dispersion

The main purpose of this subsection is to derive the upper limit of the source distance because we have to examine whether we can exclude the midnight sector (furthest possible source) as the source of the wedge-like dispersion from this best case. Derivation of the upper limit of the source distance requires derivation of the upper limit of the time-of-flight from the source and of the lower limit of the drift velocity. The time-of-flight derivation from ions coming from the same source with different velocities (V_1 and V_2) is generally formulated as [e.g., *Kletzing and Torbert*, 1994]:

$$t = (\frac{V_2}{V_1 - V_2})dt \tag{1}$$

where t is the elapsed time or the time-of-flight, and dt is the time difference between these two arrival times. Since a different energy means a different velocity or drift speed, time-of-flight is often derived from energy–time dispersed ion/electron signatures.

Let us examine the dispersion curve in Figure 5. First, both the 0.1 keV ions and 10 keV ions are found in a single dispersion curve for all spacecraft. This fact means that the eastward $\mathbf{E} \times \mathbf{B}$ drift (E is the summation of the magnetospheric (dawn-to-dusk) electric field and corotation electric field) exceeds the westward magnetic (gradient-$|B|$

and curvature) drift for all 0.1 $\sim$ 10 keV ions, and that the lower energy ions drift faster than higher energy ions in this energy range because the opposing magnetic drift speed is proportional to its energy ($\mathbf{E} \times \mathbf{B}$ drift is energy independent). Conversely, the upper cutoff of the dispersion (about 20 keV) constrains the upper limit of the effective electric field.

Second, the dispersion of the wedge-like structure is weak. From the proton data, we found only 5 $\sim$ 6 minutes difference between 0.1 keV and 10 keV for the single wedge-like structure at around 23:50 UT. Unfortunately, this information alone is not sufficient to extract a useful result because the observed dispersion is a combination of the time-of-flight effect and the spatial structure when the spacecraft velocity cannot be ignored compared to the drift velocity, like the present case. To extract the time-of-flight effect, we have to compare the particle distributions at the same location at different time observed by different spacecraft. The same location here means the same magnetic flux tube because we examine the drifting protons that fill the flux tube quickly by the north-south bouncing (as confirmed by the butterfly pitch angle distribution).

All time-of-flight analyses require that particles with different velocity (drift velocity in the present case) come from the same source region. Therefore, when comparing two spacecraft at the same location at different time, we assume that the convection is constant and it is the same for fast and slow drifting particles. Different (or variable) convection velocities between fast and slow drifting particles add an uncertainty depending on how quickly the spacecraft traversed between the trajectories of these particles.

Both numerical simulation and Viking observation demonstrate that all ions composing the wedge-like structure drift approximately in the azimuthal direction in the morning

sector as illustrated in Figure 6a [*Ebihara et al.*, 2001; *Yamauchi and Lundin*, 2006]. This is because the corotation electric field enhances the eastward drift component due to the magnetospheric dawn-to-dusk electric field. The expected drift direction has more than 45 degree angle to the Cluster trajectory even if we assume the maximum possible cross-L-shell drift at 9 MLT. Furthermore, the dominating $\mathbf{E} \times \mathbf{B}$ drift in this case is energy independent, making the trajectories of the low and high energy ions very similar. Since the opposing magnetic drift points azimuthal direction, both the low and high energy ions have the same radial component, making them on the same L-shell all the time. Therefore, the time-of-flight analysis by the inter-spacecraft comparison at the same location (same L-shell) is very reliable.

Here we compare S/C-3 with the other two spacecraft. As illustrated in Figure 6b, S/C-1 and S/C-4 traversed from lower L-shell to higher L-shell, whereas S/C-3 was approaching its perigee during 23:40-00:00 UT. S/C-3 at 00:00 UT is located at 2 degrees lower L-shell than S/C-1 or S/C-4 at 23:50 UT (S/C-4 is slightly inside of S/C-1), while S/C-3 traversed nearly the same L-shell at around 23:40 UT as those of S/C-1 and S/C4 at 23:50 UT. S/C-3 did not observe any low-energy (<1 keV) signature of the wedge-like structure at 23:40 UT. The absence of the wedge-like structure at 23:40 UT (S/C-3) at the reference L-shell in Figure 6b (denoted 0 degree) means that the wedge-like structure suddenly appeared at that L-shell at 23:50 UT (S/C-1 and S/C-4), while the same magnetic tube was empty 10 minutes earlier. This fact constrains the upper limit of the time-of-flight dispersion as <15 minutes from the fastest drifting <0.1 keV ions (at 23:40 UT) to the slowest drifting >10 keV ions (at 23:55 UT).

The small but non-zero cross-L-shell drift component causes the slow (10 keV) ions move outward (toward higher L-shell) along the spacecraft trajectory (all 9 MLT) from the L-shell where the fast (0.1 keV) ions are detected during the time-of-flight because they are in the same L-shell until the fast ions are detected. In other words, the location of S/C-3 without signature (fast ions) corresponding to the 10 keV ion signature at S/C-1 (slow ions) shifts slightly inward (i.e., later than 23:40 UT). This slightly reduces the time-of-flight, and does not affect the present discussion because we obtained the upper limit of the time-of-flight here.

The same types of time-of-flight measurement can theoretically be possible by comparing S/C-1 and S/C-4. Although S/C-1 and S/C-4 show a very similar pattern with only a few minute time lag (Figure 5), this comparison does not give a good constraint for the present case. The delay time between S/C-1 and S/C-4 traversing the same L-shell is expected to be $7 \sim 8$ minutes for quiet magnetospheric condition, but the Tsyganenko-96 model [*Tsyganenko and Stern*, 1996] predicts about $4 \sim 6$ minutes delay for the present magnetospheric condition (This difference comes from the orbital difference between these spacecraft in the north-south direction). The wedge-like structures are observed at S/C-1 and S/C-4 about 2 minutes different for oxygen and 4 minutes different for protons between these two spacecraft (Figure 5). If we take the shortest time delay between two spacecraft (4 minutes), both S/C-1 and S/C-4 observed the same energy at the same L-shell over this time delay. If we take the longest time delay (8 minutes), 0.1 keV protons in S/C-1 correspond to 10 keV protons in S/C-4 at the same L-shell. The resultant time-of-flight from <0.1 keV ions to >10 keV ions becomes from 7 minutes to infinity.

Furthermore, a time-of-flight calculation from such closely located spacecraft suffers from fluctuations of the drift direction over a short distance. The nearly azimuthal drift for all the $0.1 \sim 10$ keV is an average drift over a long distance, and is not guaranteed for the very local drift. If the short-time fluctuation of the electric field (e.g., 0.01 Hz Pc-5 range) causes a large drift in the radial direction, the slow ions are no longer at the same L-shell as the fast ions that are detected after a short time comparable to the fluctuation period. Therefore, we use a long time span, i.e., between S/C-3 and the other spacecraft, for the time-of-flight analysis.

As mentioned above, the lower energy ions drift faster as long as the drift direction is the same (eastward) inside the single dispersion. Since the dispersion is continuous for at least $0.1 \sim 10$ keV, we can set V_1 and V_2 in equation (1) as the drift speeds of 0.1 keV protons and 10 keV protons, respectively.

Using the fact that the magnetic (gradient-$|B|$ and curvature) drift velocity is proportional to the energy, i.e., 100 times faster for 10 keV ions than for 0.1 keV ions for the present case, and assuming that the ion drift is mostly defined by the $\mathbf{E}\times\mathbf{B}$ and magnetic drifts, equation (1) becomes,

$$\frac{(t+dt)}{dt} \sim \frac{V_E}{V_B} \tag{2}$$

where V_E is the eastward $\mathbf{E}\times\mathbf{B}$ drift velocity and V_B is the westward magnetic (gradient-$|B|$ and curvature) drift velocity for the last arriving (10 keV) ions.

The westward gradient-$|B|$ drift for ions with 90-degree pitch angle in the equatorial plane is given as

$$\frac{W_\perp \nabla_\perp B}{qB^2} = \frac{3W_\perp}{qRB}$$

in the dipole field, where B is the magnetic field, W is the particle energy ($\perp$ denotes perpendicular direction to the magnetic field), q is the charge of ion, and R is the distance from the Earth's dipole. The summation of the westward magnetic (gradient-$|B|$ and curvature) drift for ions with general equatorial pitch angle α is nearly the same as the limited case above, except that we have to multiply by a factor $g(\alpha) < 1$ [e.g., *Roederer*, 1970, page 57]:

$$V_B = \frac{3g(\alpha)W}{qRB}.$$

For $\alpha > 40°$, $g(\alpha) \sim 0.70 + 0.30 \sin\alpha$, and the minimum value of $g(\alpha)$ in the dipole field is 0.67 at α=0 [*Schulz*, 1971].

With this relation, the ratio of the eastward $\mathbf{E} \times \mathbf{B}$ drift to the westward gradient-$|B|$ and curvature drift is approximately

$$\frac{V_E}{V_B} = \frac{E}{B} \cdot \frac{qRB}{3g(\alpha)W} \sim \frac{2.2LE[\mathrm{mV/m}]}{\mathrm{g}(\alpha)\mathrm{W[keV]}} \tag{3}$$

where E is the effective electric field.

According to equation (3), the magnetic (gradient-$|B|$ and curvature) drift speed for 10 keV ions with pitch angle $40° < \alpha < 90°$ is comparable to the $\mathbf{E} \times \mathbf{B}$ drift speed for a few mV/m electric field depending on the equatorial pitch angle α. Applying this relation to equation (2) and using values $W = 10$ keV and $L \sim 4.5$, we finally have

$$\frac{t + dt}{dt} \sim \frac{E[\mathrm{mV/m}]}{\mathrm{g}(\alpha)}. \tag{4}$$

We now use the in situ field observations to estimate the source of the wedge-like structures. The observed magnetic field strengths are 300 $\sim$ 400 nT during this 40 minutes. The duskward components of the electric field are $-1 \sim +3$ mV/m during 23:30–00:10 UT for all spacecraft according to EFI data shown in Figure 7. During

23:40–23:50 UT, S/C-3 was near the equatorial plane (within 10° GSM latitude) and the other spacecraft are slightly above the equatorial plane ($\sim 20°$ GSM latitude). Therefore the mapping factor to the equatorial plane is nearly unity. These field values make the local $\mathbf{E} \times \mathbf{B}$ drift velocity about a few km/s, which is comparable to the gradient-$|B|$ drift for 10 keV ions trapped within the equatorial region.

The electric field can also be estimated from the average drift speed calculated from the CIS data. Within the spin plane, we obtained less than 5 km/s for $0.2 \sim 1$ keV protons when the wedge-like structure appeared. This corresponds to 2 mV/m electric field. Although this method has a larger uncertainty than EFI measurement, the good agreement between both methods indicates that the obtained electric field value (and the drift velocity) is reliable.

If we take 2 mV/m (this is slightly larger than the average value just before 23:50 UT), the right-hand side of equation (4) becomes $2 \sim 2.3$ for $\alpha > 40°$, and the maximum elapsed time before 23:40 UT becomes less than $15 \sim 20$ minutes depending on the equatorial pitch angle (90 degrees corresponds to 15 minutes). With the $\mathbf{E} \times \mathbf{B}$ drift velocity only 5 km/s in this case, the source distance is estimated as less than 1 R_E, i.e., very local. Note that this is the upper limit and that the actual value could be even smaller (the value is proportional to the separation of the spacecraft).

If we take 3 mV/m, the right-hand side of equation (4) becomes $3 \sim 3.5$ for $\alpha > 40°$, and the maximum elapsed time before 23:40 UT becomes about $30 \sim 40$ minutes with the source distance less than 3 R_E. A 3 R_E distance from 9 MLT at L=4.5 corresponds to 6.5 MLT. Considering that the given values are the upper limit, the above two estimates agree

quite well with the latest substorm onset timing at 23:10 UT (formation of the wedge-like dispersion is after this timing).

In this estimate, however, the drift could have experienced an extremely strong electric field before 23:30 UT. To examine this extreme case, we take 5 mV/m for the electric field. The right-hand side of equation (4) becomes $5 \sim 5.5$ for $\alpha > 40°$, and the maximum elapsed time before 23:40 UT becomes about $60 \sim 70$ minutes. The source distance for this case is less than 8 Re, i.e., the source location is early morning sector (>2 MLT).

For the smaller pitch angles, the ions reach low altitude and spend most of the time near the mirror point [e.g., *Alfvén and Fälthammar*, chapter 2.5]. According to Figure 5, the majority of ions that compose the stripes have a pitch angle of about 30 degrees, locating the mirror point inside the diverging part of the dipole field, i.e., where the gradient of the magnetic field is small. Then the gradient-$|B|$ drift would be even less effective than the curvature drift. In that case, the $g(\alpha)$ factor is smaller than the value given by the approximated formula, although the calculated value of $g(\alpha)$ is not very far from the approximation [*Schulz*, 1971].

Since the above estimation for $\alpha > 40°$ covers $g = 0.9 \sim 1$, we here make the same estimate for the extreme case with the minimum value g=0.67 [*Schulz*, 1971]. If we take 2 mV/m, the right-hand side of equation (4) becomes 3, and the maximum elapsed time before 23:40 UT becomes about 30 minutes with a source distance of less than 2 R_E. If we take 3 mV/m, the right-hand side of equation (4) becomes 4.5, and the maximum elapsed time before 23:40 UT becomes about 50 minutes with a source distance of less than 4 R_E. If we take 5 mV/m, the right-hand side of equation (4) becomes 7.5, and the maximum

elapsed time before 23:40 UT becomes about 100 minutes with a source distance of less than 10 Re.

The most realistic estimates using the measured electric field (2 mV/m) predict the elapsed time as less than half an hour. Such a short (less than 30 minutes) elapse time means that the averaging method over the magnetic bottle bouncing to obtain the drift speed does not always work. To see it, let us examine the oxygen data as well as pitch angle.

3.3. Oxygen behavior

In Figure 5, the oxygen (O^+) channel's wedge-like structure observed by S/C-1 and S/C-4 has two components. One is the high-energy component (>0.3 keV) that synchronizes with the proton flux. They could be ghost counts due to contaminations from protons, and we do not discuss this part. The other is the low-energy component ($0.05 \sim 0.3$ keV) that has three characteristics: (1) The low-energy oxygen ions appeared before the protons at the beginning of the wedge-like structure. (2) The pitch angle distribution for these low-energy oxygen ions has a peak in the anti-parallel direction, while the protons have ordinary symmetric butterfly distribution at 23:50 (S/C-1 and S/C-4). (3) No loss-cone is recognized for oxygen ions, whereas we can recognize the loss-cone for protons.

The butterfly pitch angle distribution indicates that S/C-1 and S/C-4 went into the magnetic flux tube filled with bouncing protons, while the uni-directional field-aligned distribution suggests that these low-energy oxygen ions have just arrived to the spacecraft location. The no-reflection property of the oxygen ions supports this interpretation, and hence the low-energy ($0.05 \sim 0.3$ keV) oxygen ions at 23:50 UT must have just arrived from the northern hemisphere without experiencing mirror reflection.

The appearance of oxygen ions before protons also suggests a non-bouncing effect, although this overshoot can partly be explained by finite gyroradius effect. If the oxygen ions did not experience any bouncing, we can no longer compare the bounce-averaged proton drift and non-averaged oxygen ion drift because the distributions of the electric and the magnetic fields is normally different between the northern hemisphere and the southern hemisphere. Therefore, it is quite possible that the oxygen ions overshoot compared to the bounce-averaged location, causing the earlier arrive than the mirroring protons. This is also consistent with the difference between the 23:50 UT event (S/C-1 and S/C-4) and the 00:00 UT event (S/C-3): the oxygen ions and the protons are clearly separated in energy space at 23:50 UT while they are mixed at 00:00 UT.

Let us estimate the source distance. The no-reflection signature indicates that these oxygen ions have not been mirror-bounced, i.e., they could not complete 3/4 bounce along the geomagnetic field. Since 0.2 keV oxygen travels only 40 km/s (4 times slower than a proton), it takes about 10 minutes to travel 1/4 bounce (from one hemisphere to this region) and hence about 30 minutes to complete 3/4 bounce. Therefore, the wedge-like dispersion observed at 23:50 UT is most likely formed within 30 minutes. The oxygen energy extends down to 0.05 keV, i.e., to half the velocity as 0.2 keV oxygen ions. The 0.05 keV oxygen ions take about 20 minutes from the source to the spacecraft position. Altogether, the elapsed time is most likely about $20 \sim 30$ minutes before 23:50 UT (start time around 23:20–23:30 UT). This number agrees with the elapsed time calculated from the effective electric field 2 mV/m, an average value seen in Figure 7.

In summary, the pitch angle distribution and the dispersion signature, together with the observed electric field, strongly suggest that the observed wedge-like structure was

formed within 30 minutes before the observation of the wedge-like structure at 23:50 UT. This short time corresponds to a morning source. Again, the latest substorm started at 23:10 UT is a good candidate as the ultimate cause of this wedge-like structure.

3.4. IMAGE observations

Although the dispersion itself most likely started in the morning sector, the source ion population ($0.1 \sim 10$ keV ions) could have come from nightside by a very fast convection if the electric field in the midnight-to-morning sector is sufficiently strong (cf. scenario (B) in subsection 2.2). To provide the global context for the in situ observations, we use global energetic neutral atom (ENA) images of the ring current obtained by the High Energy Neutral Atom (HENA) imager [*Mitchell et al.*, 2000] on board the IMAGE spacecraft [*Burch et al.*, 2000]. By detecting the direction, energy, and mass of ENAs created by the charge exchange between singly charged ring current ions and the exosphere or upper atmosphere, HENA can form images of the global ring current distribution in the $10 \sim 200$ keV range for hydrogen and $50 \sim 264$ keV for oxygen, with a minimum angular resolution of 3×3 deg. This information in turn provides the electric field distribution.

The only possible substorm that could have generated the observed wedge-like structure is the one started at around 23:10 UT. The HENA observations show that indeed the ring current region experienced a substorm injection at around 23:10 UT with a preference to the post-midnight sector as shown in Figure 8. Figure 8 shows the HENA images (10 minutes integration) from 22:59 UT, 23:09 UT, and 23:50 UT. The upper row displays the images integrated over the hydrogen 27–60 keV passband; the second row over the hydrogen 60–119 keV passband, and the third row for oxygen over the 138-264 keV passband. The angular scattering in the front foil of HENA introduces a point spread in the images,

which for 27–60 keV hydrogen is about 10 degrees full width at half maximum (FWHM), for 60–119 keV hydrogen about 5 degrees FWHM, and for 138–264 keV oxygen about 20 degrees. In order to show the images as a human eye would perceive them, each image is displayed in an equi-distant azimuthal projection. Dipole field-line pairs of L-shells of 4 and 8 are plotted for reference as indicated at each local time of noon, dawn, midnight, and dusk.

The IMF was southward from about 19:30 to 20:36 UT, then primarily northward 20:36–22:50 UT, and then stayed southward for several hours. Accordingly, ENA intensities are drastically enhanced during 20:05–20:36 UT [*Brandt et al., 2002*; *Fok et al., 2003*] in the nightside, but ceased by 22:59 UT. This is a general consequence of the southward IMF due to enhanced convection. The transported plasma from the nightside via $\mathbf{E} \times \mathbf{B}$ drift into the stronger magnetic field strength around midnight, resulting in energized plasma and enhanced ion intensities around midnight.

Slightly before 23:00 UT the IMF turned strongly southward again enhancing convection and leading to the substorm at around 23:10 UT. The first signs of the substorm injection can be seen in all HENA channels at around 23:09 UT and grows gradually stronger for about 30 minutes, which could be a signature of continued convection. The oxygen channel displays a very sharp intensification at the time of the substorm onset. This intensification is due to oxygen ions being non-adiabatically energized during the substorm dipolarization and their subsequent injection into the inner magnetosphere and precipitation onto the upper atmosphere [*Delcourt, 2002*; *Mitchell et al.*, 2003; Jones et al., this issue]. The difference in behavior between oxygen ions and protons during substorms is consistent

with the difference in pitch angle distributions presented here, as well as the altitude difference reported in *Yamauchi et al.* [2005].

In the 27–60 keV hydrogen channel immediately after the substorm onset (23:09–23:19 UT), one can recognize a clear post-midnight preference, although the westward magnetic drift is normally much stronger than the eastward $\mathbf{E} \times \mathbf{B}$ drift at this energy range. This indicates that the electric field is extremely strong (nearly 10 mV/m locally), suggesting that the energy dependence of the magnetic drift below 10 keV can be ignored compared to the $\mathbf{E} \times \mathbf{B}$ drift there.

In summary, the low-energy plasma (<10 keV) could have convected to the morning sector quickly without forming the dispersion. This means that the substantial destination of the plasma injection of <10 keV ions could be the morning sector. The preference for the post-midnight sector is stronger for lower-energy ions during large magnetic storms [e.g., *Brandt et al.*, 2002; *Ebihara and Fok*, 2004].

4. Discussion

4.1. Source location and mechanism

The new Cluster statistics on the local-time dependence in section 2 (Figure 3) indicates that a substantial number of the wedge-like structures might be formed in the morning sector, as was also suggested from the Viking statistics [*Yamauchi and Lundin*, 2006]. The case study on the 21 October 2001 event in section 3 indicates that the wedge-like structure observed at 23:50 UT is most likely formed in the morning sector within half an hour before 23:50 UT. This short drift time is obtained both from the inter-spacecraft time-of-flight analyses on the protons and from the pitch angle feature of the oxygen ions.

The quick response to substorms was also suggested from the Viking statistics [*Yamauchi and Lundin* 2006].

Table 1 lists possible causes of the observed wedge-like structure on 21 October 2001. As mentioned in subsection 2.2, we can classify the scenarios into three categories in terms of the location of the energization of dispersion-free plasma source (first column) and the start location of the dispersion (second column).

The first category is that the wedge-like structure is formed in the midnight sector but could not be detected due to the orbital characteristics of the spacecraft. Since the auroral emission and related plasma region expands to nearly L=4 in this local time during substorms [e.g., *Akasofu*, 1964; *Hoffman and Burch*, 1973; *Gussenhoven et al.*, 1987], the wedge-like structure can well be located at a lower latitude than what Cluster covers. Then the wedge-like structure will be less frequently observed by Cluster.

However, this explanation does not explain the nearly immediate appearance of the edge-like structure observed by Viking. The nearly immediate appearance is confirmed from the case study on the 21 October 2001 event in the previous section (only 40 minutes after the substorm onset). Conversely, this category presumes long drifting time from the nightside because the ion drift at lower L-shell is slower than at higher L-shell if we compare the angular velocity. Therefore, we dismiss this category.

The second category is that the $\mathbf{E} \times \mathbf{B}$ convection speed in the post-midnight sector is several times faster than the usual drift speed in the morning sector. Since the detection probability is counter-proportional to the velocity, the peak of the probability is expected to lie in the morning sector, beyond which the drift begins to stagnate and the signature

begins to decay. Such a quick drift also means that some sub-keV plasma might reach the morning sector before the dispersion starts.

This scenario must assume a strong electric field [e.g., *Brandt et al.*, 2002; *Fok et al.*, 2003; *Ebihara and Fok*, 2004; *Jordanova*, 2005], and such a strong field is indeed inferred from the IMAGE/HENA data in Figure 8. The inferred electric field in the post-midnight sector for the 21 October 2001 event is strong enough to drive ∼10 keV ions quickly to the morning sector. Recent simulation studies also show that >10 keV ring current ions may drift eastward and the peak of the ion flux could occur in the morning side when the shielding electric field driven by the ring current during a magnetic storm is strong enough [*Ebihara and Fok*, 2004]. When the electric field is thus strong, we are no longer able to distinguish such convection from the substorm injection. In other words, the destination of the substorm injection is substantially the morning sector [*Yamauchi and Lundin*, 2006].

The last category is the local formation (energization) of the <10 keV ions in the morning sector. Since such a local bulk energization related to substorms has never been considered, we list several possible scenarios, e.g., (1) sudden scattering of westward drifting $5 \sim 10$ keV ring current ions; (2) sudden sputtering by ordinary ring current (either westward drifting or eastward drifting) ions; and (3) bursty heating by electromagnetic waves.

Both scattering and sputtering scenarios assume that the substorm-related electromagnetic disturbances or electromagnetic stresses interact with the ordinary ring current ions >5 keV to scatter in the morning sector. Since the field-aligned current density becomes intense in the morning sector compared to the post-midnight sector for both downward

Region 1 and upward Region 2 currents [*Iijima and Potemra*, 1978; *Woch et al.*, 1993], the electromagnetic stress indeed increases in the morning sector. Also, past satellite observations show that the morning sector is the largest source of the electromagnetic disturbances and related heatings [*Moore et al., 1999*; and references therein]. Another possible driving force is the interaction with escaping ions from the ionosphere because the ion escape also maximizes in the morning sector [*Moore et al., 1999*; and references therein].

While the scattering scenario assume direct energy scattering to create a source plasma of the wedge-like structure, the sputtering scenario assumes a pitch angle scattering into the loss cone, which makes scattered ions hit the neutral exsobase at around 200 km to sputter neutral atoms. The sputtered neutral atoms are charge exchanged to ions through the upper ionosphere. These types of stimulations of low-energy ions by the energetic ions were originally considered to explain the oxygen-rich characteristic of the wedge-like structure at low-altitudes [*Yamauchi et al.*, 1996a]. Alternatively, direct or indirect (through wave) ion energization due to the precipitation may also be possible, but this rather belongs to the last scenario.

The key question regarding these scenarios is if there is sufficient supply of the primary population, i.e., the ordinary component (>5 keV) ring current ions in the morning sector at the substorm onset. All cases in Figure 2 show that the energy flux at around 5 $\sim$ 10 keV is high, although they are clearly separated from higher energy component (>20 keV). Such a high flux of 5 $\sim$ 10 ions is often observed in the ring current region in the morning sector (cf. Figure 3). Therefore, these 5 $\sim$ 10 keV ions are most likely eastward drifting and stagnate in the morning sector. An important difference from the previous

scenario of strong electric field is that these ions could have been supplied before the recent substorm through multiple substorms during a storm. The primary ions could also be westward drifting ones with higher energy (>20 keV) in the sputtering scenario. In this case, a sufficient particle flux of energetic ions is again required in the morning sector at the substorm onset, and this is again possible during magnetic storms.

The last scenario is bursty local heatings, i.e., the substorm-related electromagnetic waves directly heat the low-altitude plasma. In fact, Viking and Cluster found many local heatings up to over 1 keV in this region [*Yamauchi et al.*, 2005, Figure 6]. There are many candidates for such local heatings in the morning sector during substorms. As mentioned above, the electromagnetic stress is larger in the morning sector than in the post-midnight sector, and the wave-related ionospheric heating is strongest in the late morning sector in the closed region. We recently found an evidence that a substorm current system (and hence the energy dissipation that heats plasma) may independently be formed in the morning sector in addition to the midnight sector [*Yamauchi et al.*, 2006]. Unfortunately, we cannot examine these scenarios from the ground-based data for the 21 October 2001 event, because the morning sector at around 0 UT lies over Siberia where we have no active high-latitude magnetometer station or ionospheric radar.

The butterfly distribution seen in Figure 2 suggests that these ions ultimately originate from a low- or mid-altitude source, which is consistent with the last two scenarios (sputtering and local energization). The morning source of the keV ions was previously suggested from the butterfly distribution itself, but not as explicitly as by the data shown in Figure 3. The butterfly distribution for the average sub-keV ions in the dayside sector was first observed by CRRES [*Collin et al.*, 1993] and the late morning preference of the

butterfly distribution was pointed out by *De Benedetti et al.* [2005]. Unfortunately, their result by itself could not identify the local time of the source because their analysis was limited to >1 keV protons (corresponding to the extended wedge-like structure in the present study), and because they did not make the evolution analyses made here and in *Yamauchi and Lundin* [2006].

Finally, one should not eliminate the possibility that two or more scenarios may operate in forming the wedge-like structure. For example, the dense sub-keV protons might appear as the result of quick drift to the morning sector, whereas the dense sub-keV oxygen ions might be generated by the sputtering mechanism.

4.2. Envelope-substructure

In Figure 4, among many stripes from sub-keV to more than 100 keV that are recognized after 23:50 UT, only the first stripe shows a clear wedge-like dispersion, whereas the subsequent vertical stripes are nearly dispersion-free. A similar difference between the first stripe and the subsequent stripes is recognized in Figure 2a; i.e., a strong dispersion is recognized in the envelope structure, whereas many weak dispersions compose the internal substructure. The envelope–substructure combination is sometimes observed regardless of the upper cutoff energy, and has even been observed since the 1970s in association with substorm particle energization/injection, e.g., by the ATS-6 satellite [*McIlwain*, 1975].

In Figure 2a, the envelope has a north-south symmetric wedge-like structure, and it is clearly a spatial one [cf. *Yamauchi et al.*, 2005]. However, the wedge-like stripes inside this envelope, i.e., the substructure, always increases their energy with increasing time; thus the structure is north-south asymmetric and a temporal one. This is a large contrast from the Viking and Freja observations in which both the envelope and substructure are spatial

ones [*Yamauchi et al.*, 1996a; 2005]. This difference should be attributed to the spacecraft velocity, i.e., the drift time of the substructure must be comparable to or shorter than the traversal time of Cluster over the ring current region.

It is quite possible that the observed series of vertical stripes in Figure 4 (up to 100 keV) could be the internal substructure of the wedge-like dispersion starting at 23:50 UT. If so, the dispersion-free feature of the substructure suggests that the vertical stripes are newly formed at a much closer distance from the spacecraft than the first dispersed strip (wedge-like structure) observed at 23:50 UT. Then, the burst of protons from 0.1 keV to over 100 keV must have been generated in the late morning sector. This reinforces the scattering and sputtering scenarios in Table 1; i.e., one should not dismiss the possibility of a local energization process up to 100 keV in the late morning sector. We need solid studies to reveal the envelope–substructure relation in the future.

5. Summary and Conclusion

We studied the wedge-like dispersed sub-keV ions (so called the wedge-like structure) using Cluster CIS data. Cluster statistics over 550 traversals (January 2001 to July 2003) using a new identification criterion shows a clear local-time dependence (Figure 3). The limited wedge-like structure (the upper energy cutoff is less than about 1 keV) is mostly found in the afternoon sector and the extended wedge-like structure (the upper energy cutoff extends to more than 1 keV) is mostly found in the morning sector. The overall probability shows a smooth distribution with the peak probability in the morning sector, which is in good agreement with the mid-altitude observations. Both types of the wedge-like structures have the butterfly pitch angle distribution. Combined with past observations [*Yamauchi and Lundin*, 2006] and simulation [*Ebihara et al.*, 2001], the

extended wedge-like structure is most likely the original form of the limited wedge-like structure.

Since both the local-time distribution and the pitch angle distribution suggest that the dispersion started in the morning sector, we also examined a case in which the wedge-like structure is formed during a single perigee traversal of Cluster, i.e., when Cluster shows a clear inbound-outbound asymmetry. The clearest asymmetry over the first 3 years of Cluster operation took place on 21 October 2001. Dense protons at a wide energy range ($0.1 \sim 10$ keV) suddenly appeared as a single energy dispersion curve at 23:50 UT during the outbound traversal, although no signature is observed at 23:40 UT in the same magnetic flux tube. The wide energy range of the dispersion to over 10 keV directly means that the $\mathbf{E} \times \mathbf{B}$ drift is stronger than the magnetic (gradient-$|B|$ and curvature) drift even for 10 keV ions.

Multi-spacecraft analyses of the dispersion curve shows that the drift time difference between 0.1 keV protons and 10 keV protons is less than 15 minutes for the suddenly appearing wedge-like structure at 23:50 UT. Considering the electric field measurement of <3 mV/m duskward component which is obtained both from EFI data and drift calculation from CIS data, the source distance is most likely less than 3 R_E with a travel time of less than half an hour before 23:50 UT when the wedge-like structure was first detected.

This result (elapsed time) is also supported by the nearly simultaneous appearance of the low-energy ($0.05 \sim 0.3$ keV) oxygen ions with protons. The pitch angle distributions are different between the low-energy protons (symmetric butterfly distribution) and low-energy oxygen ions (mostly in the anti-parallel direction without reflection signature), indicating that those low-energy oxygen ions came from the northern hemisphere and did

not have time to be mirrored back in the southern hemisphere. The earlier appearance of oxygen ions than protons can also be explained by the difference between the bounce-averaged drift speed (for protons) and non-averaged speed (for oxygen ions). Since 0.2 keV oxygen ions are not mirror-reflected and since oxygen ions with an energy down to 0.05 keV are detected, the elapsed time is estimated as about $20 \sim 30$ minutes.

Thus, Cluster data indicates that the dispersion of the wedge-like structure and the oxygen ion ejection began in the morning sector mainly in the northern hemisphere at around 23:20–23:30 UT. The responsible substorm must be the one that began at around 23:10 UT. According to IMAGE/HENA data, 27–60 keV protons drifted eastward in the post-midnight sector, indicating that the electric field could be very strong (up to 10 mV/m) right after the substorm onset. Such a strong electric field may drive 10 keV ions to the morning sector very quickly.

Finally, we proposed several scenarios that can explain the observation (Table 1). Since all scenarios are possible at present, we need further studies to pinpoint the correct ones.

Acknowledgments. The Cluster project is carried out by ESA and the Cluster 2 CIS instrument was supported by ESA and build by many institutions: CESR Toulouse as PI institute, IRF Kiruna, MPE Garching, IFSI Roma. MPAE (now MPS) Lindau, U Bern, U Washington, UNH, LPARL, and UCB/SSL. The other Cluster data (RAPID, EFI, FGM, and orbit) are obtained through the Cluster Science Data System. IMAGE mission is supported by NASA. Work at IRF Kiruna (MY, HN, and RL) is supported by Swedish Space Board and Swedish Research Council. Work at JHU/APL (PB) is supported by NASA grant NAG5-12722 and NSF grants ATM-0302529. MY thanks programs for disabled people in Sweden which have made it possible for him to work.

References

Akasofu, S.-I. (1964), The development of the auroral substorm, *Planet. Space Sci., 12*, 273.

Alfvén, H. and C.G. Fälthammar (1963), *Cosmical Electrodynamics*, Clarendon, Oxford.

Burch, J.L. (2000), IMAGE mission overview, *Space Sci. Rev.*, *91*(1-2), 1–14.

Brandt, P. C., S. Ohtani, D. G. Mitchell, M.-C. Fok, E. C. Roelof, and R. Demajistre (2002), Global ENA observations of the storm mainphase ring current: Implications for skewed electric fields in the inner magnetosphere, *Geophys. Res. Lett.*, *29*(20), 1954, doi:10.1029/2002GL015160.

De Benedetti, J., A. Milillo, S. Orsini, A. Mura, E. De Angelis, and I.A. Daglis (2005), Empirical model of the inner magnetosphere H+ pitch angle distribution, in *The Inner Magnetosphere: Physics and Modeling*, edited by T.I. Pulkkinen, N.A. Tsyganenko, and R. Friedel, AGU Monoraph, pp. 283–291.

Delcourt, D.C. (2002), Particle acceleration by inductive electric fields in the inner magnetosphere, *J. Atm. Solar-Terr. Phys.*, *64*, 551–559.

Ebihara, Y., M. Yamauchi, H. Nilsson, R. Lundin, and M. Ejiri (2001), Wedge-like dispersion of sub-keV ions in the dayside magneto-sphere: Particle simulation and Viking observation, *J. Geophys. Res.*, *106*, 29571–29584.

Ebihara, Y., and M.-C. Fok (2004), Postmidnight storm-time enhancement of tens-of-keV proton flux, *J. Geophys. Res.*, *109*, A12209, doi:10.1029/2004JA010523.

Fok, M.-C., T.E. Moore, G.R. Wilson, J.D. Perez, X.X. Zhang, P. C.Brandt, D.G. Mitchell, E.C. Roelof, J.-M. Jahn, C.J. Pollock and R.A. Wolf (2003), Global ENA IMAGE simulations, *Space Sci. Rev.*, *109*(1-4), 77–103.

Gussenhoven, M.S., D.A. Hardy, and N. Heinemann, The equatorward boundary of auroral ion precipitation, *J. Geophys Res.*, *92*(A4), 3272–3283, 1987.

Hoffman, R.A., and J.L. Burch (1973), Electron precipitation patterns and substorm morphology, *J. Geophys. Res.*, *78*(16), 2867–2884.

Iijima, T., and T. A. Potemra (1978), Large-scale characteristics of field-aligned currents associated with substorms, *J. Geophys. Res.*, *83*, 599–615.

Jordanova, V.K. (2005), Source, transport, and losses of energetic particles during geomagnetic storms, in *The Inner Magnetosphere: Physics and Modeling*, edited by T.I. Pulkkinen, N.A. Tsyganenko, and R. Friedel, AGU Monoraph, pp 9–21.

Kletzing, C.A., and Torbert, R.B.(1994), Electron time dispersion, *J. Geophys. Res.*, *99*, 2159–2172.

McIlwain, C.E. (1974), Substorm injection boundaries, in *Magnetospheric Physics*, edited by B.M. McCormac, D. Reidel, Dordrecht, Holland, pp. 143–154.

McIlwain, C.E. (1975), Auroral electron beams near the magnetic equator, in *Physics of the hot plasma in the magnetosphere*, edited by B. Hultqvist and L. Stenflo, Prenum, New York, pp. 91–112.

Mitchell, D.G., S.E. Jaskulek, C.E. Schlemm, E.P. Keath, R.E. Thompson, B.E. Tossman, J.D. Boldt, J.R. Hayes, G.B. Andrews, N. Paschalidis, D.C. Hamilton, R.A. Lundgren, E.O. Tums, P. Wilson, H.D. Voss, D. Prentice, K.C. Hsieh, C.C. Curtis, F.R. Powell (2000), High energy neutral atom (hena) imager for the IMAGE mission, *Space Sci. Rev.*, *91*(1-2), 67

Mitchell, D. G., P. C.Brandt, E.C. Roelof, D.C. Hamilton, K.C. Retterer, and S. Mende (2003), Global imaging of O+ from IMAGE/HENA, *Space Sci. Rev.*, *109*, 63–75

Moore, T.E., Lundin, R., Alcayde, D., Andre, M., Ganguli, S.B., Temerin M., and Yau, A. (1999), Source processes in the high-latitute ionosphere, Chapter 2 in *Magnetospheric Plasma Sources and Losses*, edited by B. Hultqvis et al., Kluwer Academic Pub., pp. 7–84.

Newell, P.T., and C.-I. Meng (1986), Substorm introduction of 1 keV magne-tospheric ions into the inner plasmasphere, *J. Geophys. Res.*, *91*, 11133–11145.

Newell, P. T., and C.-I. Meng (1992), Mapping the dayside ionosphere to the magnetosphere according to particle precipitation characteristics, *Geophys. Res. Lett*, *19*, 609–612.

Rème, H., C. Aoustin, J.M. Bosqued, I. Dandouras, B. Lavraud, et al. (2001), First multispacecraft ion measurements in and near the Earth's magnetosphere with the identical Cluster ion spec-trometry (CIS) experiment, *Ann. Geophys.*, *19*, 1303–1354.

Roederer, J.G. (1970), *Dynamics of Geomagnetically Trapped Radiation*, Springer-Verlag, New York.

Potemra, T. A. (1994), Sources of large-scale Birkeland currents, in *Physical signatures of magnetospheric boundary layer process*, edited by J. A. Holtet, and A. Egeland, 3-27, Kluwer Academic Publishers, Dordrecht, Netherlands.

Sauvaud, J.A., J. Crasnier, K. Mouala, R.A. Kovrazhkin, and N.V. Jorjio (1981), Morning sector ion precipitation following substorm in-jections, *J. Geophys. Res.*, *86*, 3430–3438.

Schulz M. (1971) Approximate Second Invariant for a Dipole Field, *J. Geophys. Res*, *76*, 3144.

Tsyganenko, N.A. and D.P. Stern (1996), A new generation global magnetosphere field model, based on spacecraft magnetometer data, *ISTP newsletter*, *6*(1), 21.

Vallat, C. (2004), *Etude du Courant Annulaire de la Magnétosphre Terrestre á l'aide des données obtenues á bord des quatre satellites du projet CLUSTER* (French text with English absstract), Ph.D Thesis, Paul Sabatier University, Toulouse, December 2004, 218 pp.

Woch, J., M. Yamauchi, R. Lundin, T. A. Potemra, and L. J. Zanetti (1993), The low-latitude boundary layer at mid-altitudes: Relation to large-scale Birkeland currents, *Geophys. Res. Lett.*, *20*, 2251–2254.

Yamauchi, M., R. Lundin, L. Eliasson, and O. Norberg (1996a), Meso-scale structures of radiation belt/ring current detected by low-energy ions, *Adv. Space Res.*, *17*(2), 171–174.

Yamauchi, M., R. Lundin, K. Mursula, G. Marklund, and T. A. Potemra (1996b), Dayside Pc5 pulsation detected by Viking ion data at L=4, *Geophys. Res. Lett.*, *23*, 2517–2520.

Yamauchi, M., R. Lundin, L. Eliasson, D. Winningham, H. Rème, C. Vallat, I. Dandouras, and Cluster-CIS team (2005), Structures of sub-keV ions inside the ring current region, in *The Inner Magnetosphere: Physics and Modeling*, edited by T.I. Pulkkinen, N.A. Tsyganenko, and R. Friedel, AGU Monoraph, pp. 41–46.

Yamauchi, M., and R. Lundin (2006), Sub-keV ring current ions as the tracer of substorm injection, *Ann. Geophys.*, *24*, 355–366. SRef-ID: 1432-0576/ag/2006-24-355.

Yamauchi, M., T. Iyemori, H. Frey, and M. Henderson (2006), Unusually Quick Development of 4000 nT Substorm During Initial 10 Minutes of 29 October, 2003 Magnetic Storm, *J. Geophys. Res.*, *111*, A04217, doi:10.1029/2005JA011285.

Figure 1. Energy–time ion energy flux spectrograms for (a) Viking positive ion data (17 July 1986) and (b) Cluster CIS/CODIF proton data (21 August 2001). The Viking data (0.05–1.2 keV) is taken from one direction which scans 2π pitch angles (sun-pulse is seen at a oblique pitch angle) every 20 seconds. The Cluster data (0.05–10 keV) is integrated over all 4π direction. The wedge-like energy–latitude sub-keV ions are marked by arrows: they are recognized between 61–68 invariant latitudes (ILat) in the Viking data and between 1–3 R_E (Earth radius) in Geo-Solar-Ecliptic (GSE) Z coordinate in the Cluster data

Figure 2. Energy flux observed by Cluster CIS/CODIF instrument (spacecraft 4 only). From top to bottom: energy–time spectrogram for 0.03–40 keV proton from all direction, pitch angle–time spectrogram for 0.2–1 keV proton, pitch angle–time spectrogram for 5–40 keV proton, and energy–time spectrogram for 0.03-40 keV oxygen ion from all 4π direction. The energy flux is integrated over 4π direction and the unit is keV$\cdot$cm^{-2}s^{-1}keV^{-1}. The black-and-white scale is set to extract the dispersion patterns in the sub-keV range, and therefore $>$ 10 keV ions are saturated. The Cluster spacecraft traverse the ring current region during its perigee traversals.

Figure 3. Probability (%) of detecting clear wedge-like dispersed sub-keV ions at different MLT sectors observed by Cluster CIS instruments during two and half year period (January 2001 to July 2003). "Limited" wedge-like structure means that it is separated from the energetic component during the entire traversals (Figure 2a), and "extended" wedge-like structure means that its energy reaches to the energy of ordinary population of the ring current (> several keV) at somewhere (cf. Figure 2b and 2c). Numbers at the top of each bar is the total number of traversals in each 3-hours bin. The probability of observing the extended wedge-like structure (black part) is given above the probability of observing the limited wedge-like structure (dark grey part), so that the value of the top of the dark part represents the total probability to observe either of two types. The probability of less clear structure ("weak") is added to show the uncertainty of our statistics.

Figure 4. (Color version is found in Plate 1.) The same as Figure 2 except that energy–time spectrograms for 0.03–40 keV proton from spacecraft 1 and 3 are added on the top, and that line plots of energetic proton flux (from RAPID instrument) are add at the bottom.

Figure 5. (Color version is found in Plate 1.) Energy–time energy flux spectrograms (0.05–10 keV for both proton and oxygen ions) and pitch angle–time energy flux spectrograms (0.2–1 keV for proton and 0.1–0.5 keV for oxygen ions) observed by Cluster CIS/CODIF instruments from 23:30 UT, 21 October 2001 to 00:20 UT next day (50 minutes total). From top to bottom: spacecraft-1, spacecraft-3, and spacecraft-4.

Figure 6. Schematic drawing of relative position of Cluster with respect to the magnetic flux tube during the perigee traversal of 21–22 October 2001. Dotted lines represent meshes of coordinate and solid lines represent the spacecraft traversals. (a) Approximate Cluster position viewed in L–MLT coordinates (approximately from the north). The dot-dashed lines illustrate the drifting front of the wedge-like structure [cf. *Ebihara et al.*, 2001]. All spacecraft are located at the same MLT (within a few degrees difference). The cross-shell component of the drift speed due to the dawn-to-dusk electric field is outward but it is very small compared to the eastward component because of the corotation electric field. (b) More detailed position of each spacecraft viewed in L-Z coordinate (approximately from 15 MLT toward 3 MLT) at 23:40 UT, 23:50, UT, 24:00 UT on 21 October 2001. The relative latitude is given with the offset taken from the S/C-3 location at 23:50 UT, and this is about the same for both the dipole model and the Tsyganenko-96 model. "Yes" and "No" mean the appearance of the wedge-like structure.

Figure 7. Duskward component of DC electric field observed by Cluster EFI instruments from 23:00 UT, 21 October 2001 to 00:20 UT next day (80 minutes total). Since S/C is nearly half an hour behind the other spacecraft, the ULF-range time variation (period of $5 \sim 10$ minutes) is temporal variation at this local time (9 MLT).

Figure 8. (Color version is found in Plate 2.) ENA images of the ring current obtained by IMAGE/HENA between 22:59–23:50 UT on the 21 October 2001. Each image is obtained from a northern vantage point and the dipole field lines of L-shells 4 and 8 are drawn at noon, dusk, midnight and dawn as indicated. All images were integrated during 10 min with the start time of integration as indicated. The substorm injection takes place at around 23:10 UT as the enhancement of the ENA intensity coming from the nightside (left).

Table 1. Source of the wedge-like dispersion

keV ions	dispersion	possible scenarios
(A) nightside	nightside	no
(B) nightside	morning	strong E
(C) morning	morning	scattering, sputtering, heating

Figure 9. Color version of Figures 4 and 5

Figure 10. Color version of Figure 8

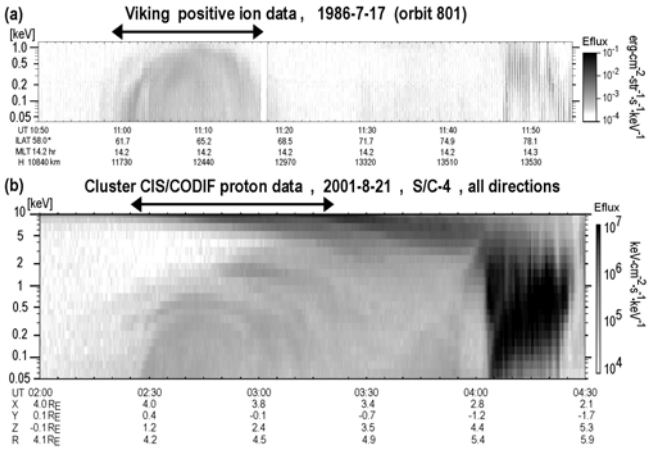

Figure 1: Energy-time ion energy flux spectrograms for (a) Viking ion data (17 July 1986) and (b) Cluster CIS/CODIF proton data (21 August 2001). The Viking data (0.05-1.2 keV) is taken from one direction which scans 2π pitch angles (sun-pulse is seen at nearly 45 degree angle) every 20 second. The Cluster data (0.05--10 keV) is integrated from all 4π direction. The wedge-like energy-latitude sub-keV ions are marked by arrows: they are can be recognized between 61-68 invariant latitudes (ILat) in the Viking data and between 1-3 RE (Earth radius) in Geo-Solor-Ecliptic (GSE) Z coordinate

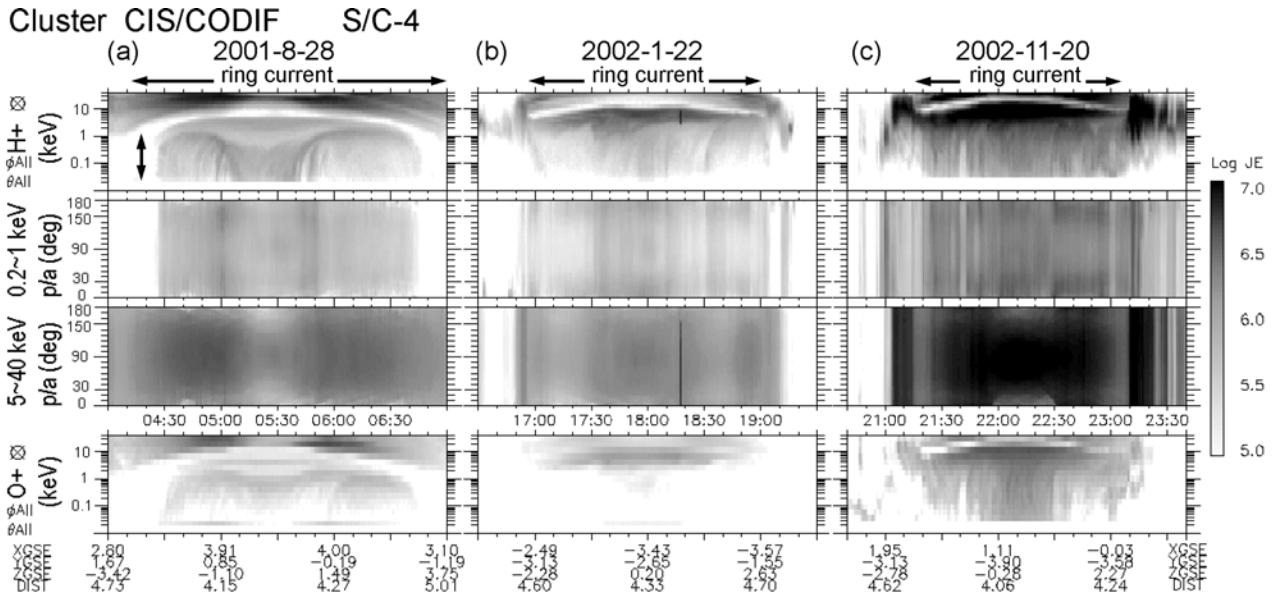

Figure 2: Energy flux observed by Cluster CIS/CODIF instrument (spacecraft 4 only). From top to bottom: energy-time spectrogram for 0.03-40 keV proton from all direction, pitch angle-time spectrogram for 0.2-1 keV proton, pitch angle-time spectrogram for 5-40 keV proton, and energy-time spectrogram for 0.03-40 keV oxygen ion from all 4π direction. The energy flux is integrated over 4π direction and the unit is $keV \cdot cm^{-2}s^{-1}keV^{-1}$. The black-and-white scale is set to extract the dispersion patterns in the sub-keV range, and therefore >10 keV ions are saturated. The Cluster spacecraft traverse the ring current region during its perigee traversals.

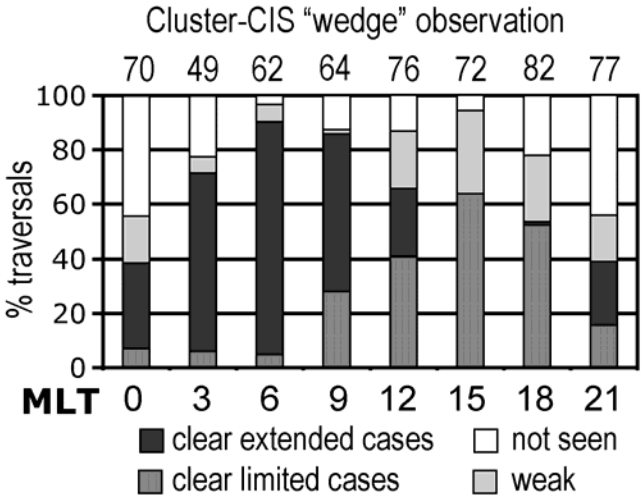

Figure 3: {Probability (%) of detecting clear wedge-like dispersed sub-keV ions at different MLT sectors observed by Cluster CIS instruments during two and half year period (January 2001 to July 2003). "Limited" wedge-like structure means that it is separated from the energetic component during the entire traversals (Figure 2a), and "extended" wedge-like structure means that its energy reaches to the energy of ordinary population of the ring current (> several keV) at somewhere (cf. Figure 2b and 2c). Numbers at the top of each bar is the total number of traversals in each 3-hours bin. The probability of observing the extended wedge-like structure (black part) is given above the probability of observing the limited wedge-like structure (dark grey part), so that the value of the top of the dark part represents the total probability to observe either of two types. The probability of less clear structure ("weak") is added to show the uncertainty of our statistics.

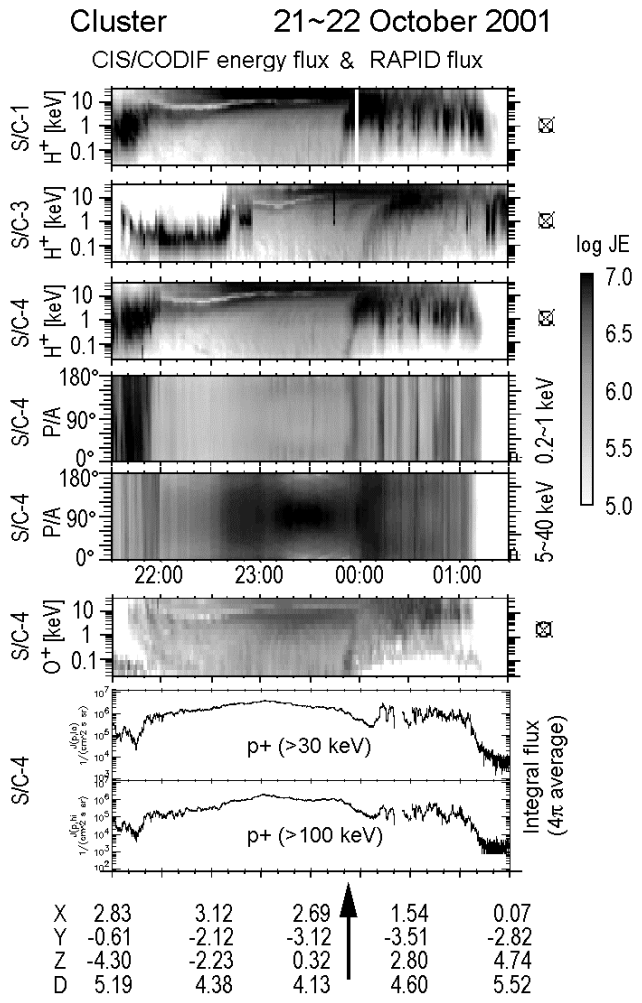

Figure 4: (Color version is found in Plate 1.) The same as Figure 2 except that energy-time spectrograms for 0.03-40 keV proton from spacecraft 1 and 3 are added on the top, and that line plots of energetic proton flux (from RAPID instrument) are add at the bottom.

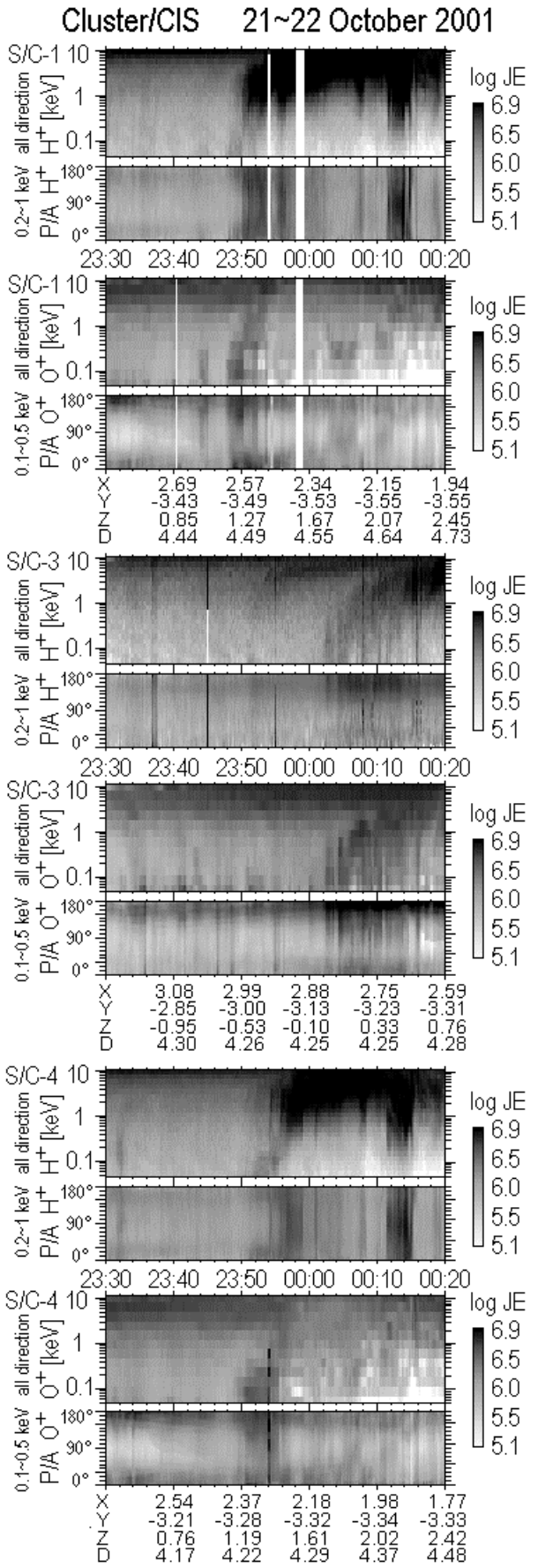

Figure 5: (Color version is found in Plate 1.) Energy-time energy flux spectrograms (0.05-10 keV for both proton and oxygen ions) and pitch angle-time energy flux spectrograms (0.2-1 keV for

proton and 0.1-0.5 keV for oxygen ions) observed by Cluster CIS/CODIF instruments from 23:30 UT, 21 October 2001 to 00:20 UT next day (50 minutes total). From top to bottom: spacecraft-1, spacecraft-3, and spacecraft-4.

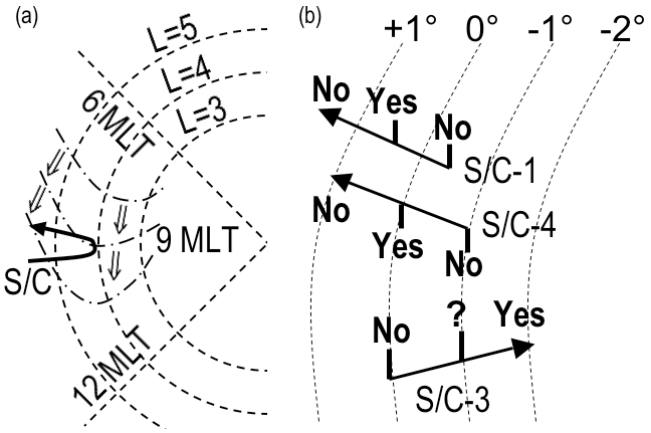

Figure 6: Schematic drawing of relative position of Cluster with respect to the magnetic flux tube during the perigee traversal of 21-22 October 2001. Dotted lines represent meshes of coordinate and solid lines represent the spacecraft traversals. (a) Approximate Cluster position viewed in L-MLT coordinates (approximately from the north). The dot-dashed lines illustrate the drifting front of the wedge-like structure [cf. *Ebihara et al*., 2001]. All spacecraft are located at the same MLT (within a few degrees difference). The cross-shell component of the drift speed due to the dawn-to-dusk electric field is outward but it is very small compared to the eastward component because of the corotation electric field. (b) More detailed position of each spacecraft viewed in L-Z coordinate (approximately from 15 MLT toward 3 MLT) at 23:40 UT, 23:50, UT, 24:00 UT on 21 October 2001. The relative latitude is given with the offset taken from the S/C-3 location at 23:50 UT, and this is about the same for both the dipole model and the Tsyganenko-96 model. "Yes" and "No" mean the appearance of the wedge-like structure.

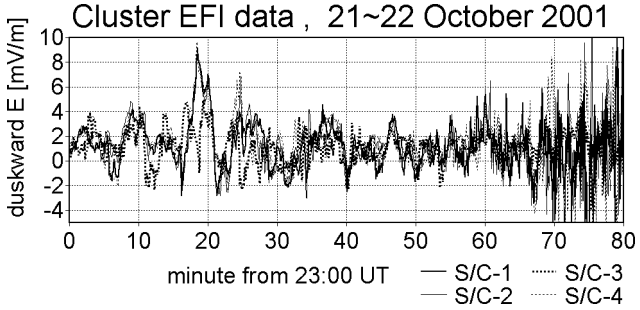

Figure 7: Duskward component of DC electric field observed by Cluster EFI instruments from 23:00 UT, 21 October 2001 to 00:20 UT next day (80 minutes total). Since S/C is nearly half an hour behind the other spacecraft, the ULF-range time variation (period of 5-10 minutes) is temporal variation at this local time (9 MLT).

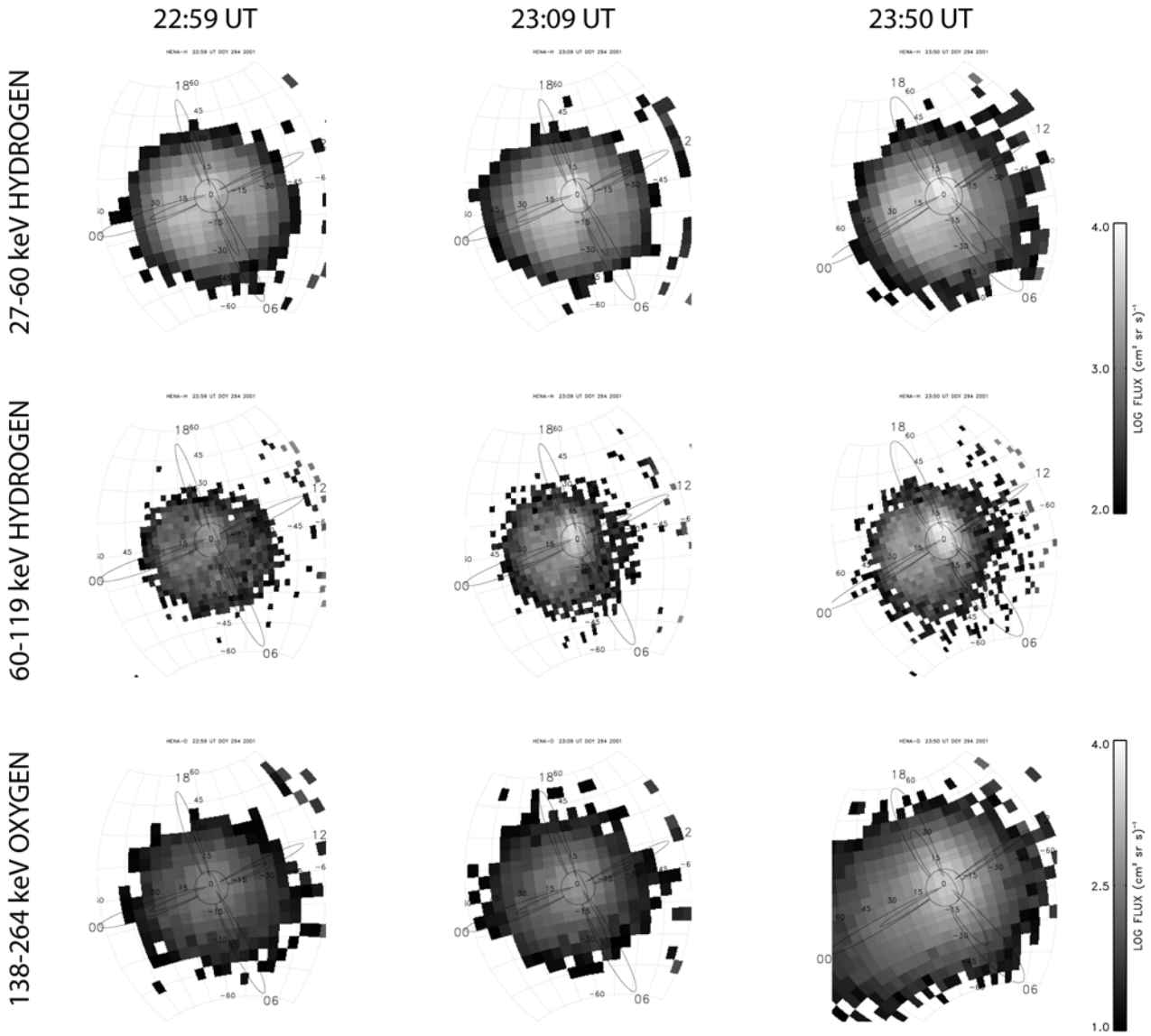

Figure 8: (Color version is found in Plate 2.) ENA images of the ring current obtained by IMAGE/HENA between 22:59-23:50 UT on the 21 October 2001. Each image is obtained from a northern vantage point and the dipole field lines of L-shells 4 and 8 are drawn at noon, dusk, midnight and dawn as indicated. All images were integrated during 10 min with the start time of integration as indicated. The substorm injection takes place at around 23:10 UT as the enhancement of the ENA intensity coming from the nightside (left).

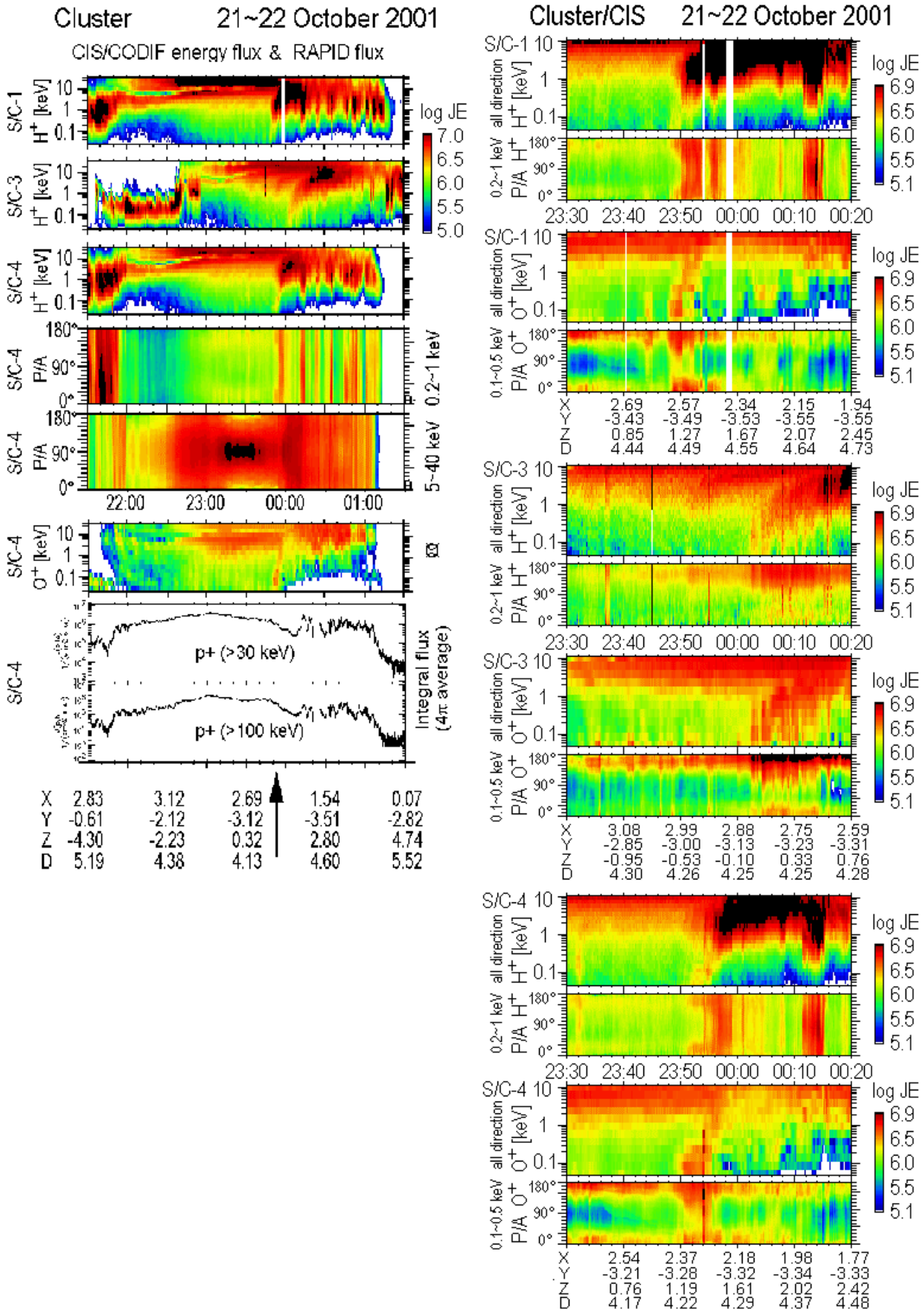

Plate 1: Color version of Figures 4 and 5

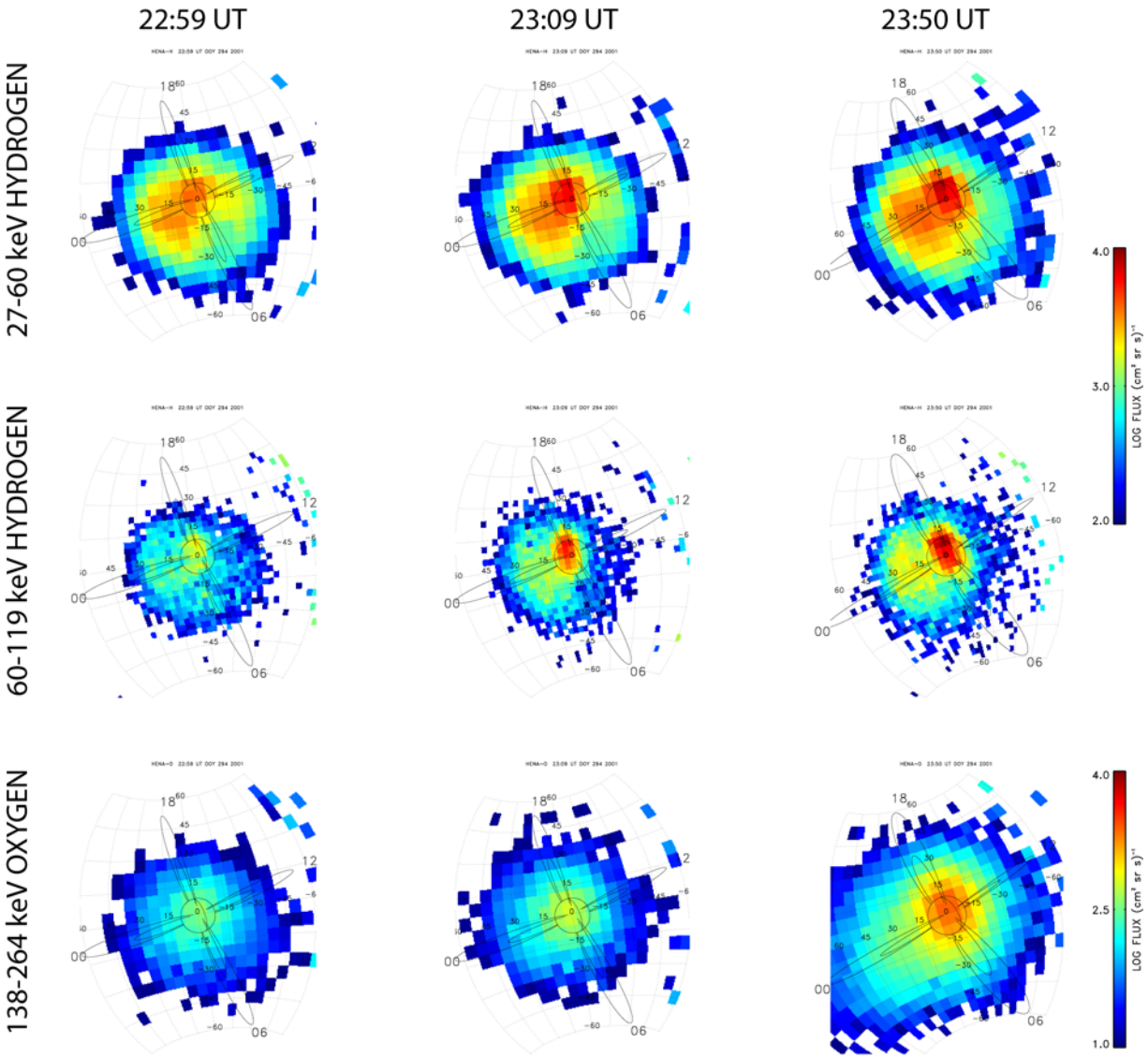

Plate 2: Color version of Figure 8